unpredicted the experimental reattachment length ($x_r/h = 12.3$) by about 15% owing to the combined effect of inadequacies of the k–ε model and numerical diffusion associated with UDS in such flows.[2–4] In the backward-facing step[11] and the bluff plate[4] cases, k–ε predictions are improved by invoking higher order schemes but still yield reattachment lengths shorter than experimental values. In contrast, in the rib flow considered here k–ε/QDS computations overpredict the reattachment length by about 8%, as shown in Fig. 2. The better agreement in this case is fortuitous and is the result of the more complex flow associated with the presence of two primary separation bubbles. The underpredicted upstream separation bubble causes an underretarded flow immediately upstream of the second separation. This results in artificially higher momentum fluxes in the shear layer separating from the upstream edge, thereby compensating for the overdiffusive properties of the k–ε model; the net effect is an overpredicted reattachment length. The values predicted by the MS turbulence model with QDS converge to within 1% of the experimental value. A small secondary recirculation zone behind the rib is obtained with the fine grid QDS computations.

Various flow zones can be identified in the wall shear stress distributions presented in Fig. 3. The distributions obtained from the k–ε and MS models show significant differences on top of and downstream from the rib. The upstream separation region is almost nonexistent in the k–ε predictions, and the magnitudes of the shear stress are lower than those of the MS model because of the over diffusive properties of the k–ε model.

The predicted longitudinal velocity profiles are compared in Fig. 4 to available measurements. The upstream profiles (at $x/h = -2.0$) are almost identical for both models and show a distribution similar to that of fully developed turbulent flow. At $x/h = -0.4$, the effect of the adverse pressure gradients caused by the obstacle becomes more prominent and the two models start deviating noticeably, with the MS model showing better agreement with measurements. The maximum reverse velocity shortly after separation on the top surface of the rib ($x/h = 0.25$) is overestimated by the MS turbulence model, while the zero mean velocity line passes through $0.23h$ above the trailing edge of the rib compared to the experimental value of $0.3h$. Overall, improved predictions with the MS model are obtained throughout. However, the first profile in the recovery zone ($x/h = 13$), though better predicted by the MS turbulence model, is not entirely satisfactory. The excessive retardation of the boundary layer in the recovery region is a discrepancy common to all available EVM and Reynolds stress model computations of reattaching flows.

An important parameter in the MS model is the turbulent kinetic energy generation-to-dissipation ratio (G_k/ε_t). This ratio determines the location of the variable partitioning of the energy spectrum, which is central to the capabilities of the MS model in resolving nonequilibrium fields. The computed contour lines of the ratio G_k/ε_t in Fig. 5 show peak nonequilibrium state associated with large turbulent kinetic energy production around the upstream edge of the rib. The ability of the MS model to resolve turbulence dynamics in this region yields less damping and hence improved predictions of the downstream flow.

Acknowledgments

The financial support of the Natural Sciences and Engineering Research Council of Canada (Grant OGP0105723) and the University of Victoria is gratefully acknowledged.

References

[1]Kessler, R., Perić, M., and Sheuerer, G., "Solution Error Estimation in Numerical Prediction of Turbulent Recirculating Flows," *Validation of Computational Fluid Dynamics*, AGARD CP 437, 1988, pp. 9.1–9.12.

[2]Bergeles, G., and Athanassiadis, N., "Numerical Study of the Flow Around a Surface-Mounted Prism," *Proceedings of Symposium on Refined Modelling of Flows* (Paris, France), 1982, pp. 47–57.

[3]Benodekar, R. W., Goddard, A. G. H., Gosman, A. D., and Issa, R. I., "Numerical Prediction of Turbulent Flow over Surface-Mounted Ribs," *AIAA Journal*, Vol. 23, No. 3, 1985, pp. 359–366.

[4]Djilali, N., Gartshore, I. S., and Salcudean, M., "Turbulent Flow Around a Bluff Rectangular Plate, Part II: Numerical Predictions," *Journal of Fluids Engineering*, Vol. 113, 1991, pp. 60–67.

[5]Hanjalić, K., Launder, B. E., and Schiestel, R., "Multiple-Time-Scale in Turbulence Transport Modeling," *Turbulent Shear Flows 2*, Springer–Verlag, Berlin, 1980, pp. 36–49.

[6]Kim, S.-W., and Chen, C. P., "A Multiple-Time-Scale Turbulence Model Based on Variable Partitioning of the Turbulent Kinetic Energy Spectrum," *Numerical Heat Transfer B*, Vol. 16, 1989, pp. 193–211.

[7]Zeidan, E., Ph.D. Thesis, Dept. of Mechanical Engineering, Univ. of Victoria, BC, Canada, 1995.

[8]Crabb, D., Durão, D. F. G., and Whitelaw, J. H., "Velocity Characteristics in the Vicinity of a Two-Dimensional Rib," *Proceedings of the 4th Brazilian Congress of Mechanical Engineering* (Florianopolis, Brazil), 1977, pp. 415–428.

[9]Leonard, B. P., "Elliptic Systems: Finite Difference Method IV," *Handbook of Numerical Heat Transfer*, Wiley, New York, 1988, pp. 347–378.

[10]Lai, K. Y. M., and Salcudean, M., Internal Rept., Dept. of Mechanical Engineering, Univ. of Ottawa, ON, Canada, 1985.

[11]Lein, F. S., and Leschziner, M. A., "Upstream Monotonic Interpolation for Scalar Transport with Application to Complex Turbulent Flows," *International Journal for Numerical Methods in Fluids*, Vol. 19, 1994, pp. 527–548

Comparison of Baldwin–Lomax Turbulence Models for Two-Dimensional Open Cavity Computations

Chung-Jen Tam,* Paul D. Orkwis,†
and
Peter J. Disimile‡
University of Cincinnati, Cincinnati, Ohio 45221-0070

Introduction

THE presence of a cavity in a surface bounding a fluid flow can cause large pressure, velocity, and density fluctuations in its vicinity, as well as propagating acoustic waves. In addition, the drag on the surface can be altered and structural failure due to resonance can occur. A persistent problem with the numerical simulation of cavity flow is the choice of an appropriate turbulence model. Many researchers have opted for the simplicity of the Baldwin–Lomax algebraic model, although many modifications to its basic form have been employed. Suhs[1] applied the standard Baldwin–Lomax model above the up- and downstream flat plates and bottom wall of the cavity, while assuming laminar flow in the region above the cavity. Rizzetta[2] used the Baldwin–Lomax model with the relaxation model[3] for three-dimensional supersonic open cavity flows. Baysal et al.[4] have researched supersonic open cavity flows using the Baldwin–Lomax turbulence model and a combination of the relaxation modification, the Degani and Schiff[5] first peak modification, and the multiple-wall modification.

Although many turbulence model modifications for cavity flowfields have been proposed, little evidence has been offered as to the suitability of a particular choice. Time-averaged surface pressure data appear to agree quite well for all models but, apparently, different flowfield behavior has been reported. This Note presents the numerical results[6] of a two-dimensional open cavity flowfield study that employed the double thin-layer Navier–Stokes equations and various versions of the Baldwin–Lomax algebraic turbulence models, including the upstream relaxation,[2,4] first peak,[4] multiple-wall,[4]

Presented as Paper 95-0361 at the AIAA 33rd Aerospace Sciences Meeting, Reno, NV, Jan. 11–14, 1995; received Jan. 30, 1995; revision received April 24, 1995; accepted for publication May 18, 1995.

*Research Assistant. Member AIAA.

†Assistant Professor of Aerospace Engineering and Engineering Mechanics. Senior Member AIAA.

‡Associate Professor of Aerospace Engineering and Engineering Mechanics. Member AIAA.

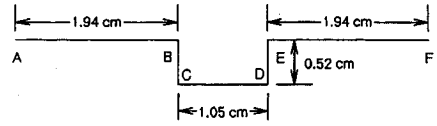

Fig. 1 Cavity geometry.

Suhs,[1] and inverse approximation of Suhs,[6] as well as two laminar flow approaches. The inverse Suhs approach consists of the Baldwin–Lomax turbulence model applied above the up- and downstream flat plates and above the cavity, with no turbulence model in the cavity itself. The first laminar flow case utilized the Baldwin–Lomax model only above the up- and downstream flat plates, and the second employed laminar flow everywhere in the computational space. The results are compared to the experimental data of Disimile and Orkwis.[7]

Governing Equations

The unsteady Reynolds-averaged, double thin-layer Navier–Stokes (DTLNS) equations were discretely solved in this work. The DTLNS equations retain the thin-layer viscous terms in both the x and y directions as opposed to the thin-layer Navier–Stokes (TLNS) equations which retain terms only in the y direction. The TLNS equations have been described by many researchers,[8,9] and as such they will not be included here. The governing equations were solved using a DTLNS modification of the implicit approximate factorization scheme of Simpson and Whitfield.[9] This scheme is second-order accurate in both time and space, and employs a Newton-like subiteration procedure. Four subiterations were used in each global iteration with a time step such that the maximum Courant–Friedrichs–Lewy (CFL) was 0.1.

Initial/Boundary Conditions

Boundary conditions were obtained from a flat plate computation that matched the experimental wind-tunnel wall boundary-layer momentum thickness θ as discussed by Orkwis et al.[10] The cavity shown in Fig. 1 was tested with flowfield conditions $M_\infty = 2$, $Re_\theta = 3.69 \times 10^4$ and $\theta = 0.979$ mm. Initially, the flow above the cavity was set equal to the flat plate solution at the location matching the experimental value of θ. The nondimensional initial conditions within the cavity were density and pressure set equal to the wall values, $\rho u = 0.5$, $\rho v = \rho w = 0.0$, and total energy defined from these quantities.

Results and Discussion

The results are grouped into surface and field properties. The surface properties include time averages of pressure and sound pressure level. Field properties are presented in the form of streamline contours. Comparison of the surface pressure frequency content was performed in an earlier work.[6]

The block grid dimensions for this study were 66×55, 66×120, and 66×55 for the upstream, cavity, and downstream blocks, respectively, with points clustered along all walls. This choice was based on a grid resolution study, the results of previous researchers, and available computational resources. Half and double x and y direction grid point densities were tested, and the fine grid results were only marginally different.

Surface Properties

Figure 2 is a comparison of the time-averaged surface pressures obtained from the experiment and the tested turbulence models. The general results can be grouped according to their performance on the forward/bottom walls and the aft wall. The best performers for one case were the worst performers for the other. For example, the best models for the front and bottom walls were the standard Baldwin–Lomax (SBL), inverse Suhs (ISU), fully laminar (FL), laminar in and above the cavity (LIA), relaxation (REL), and first peak (FP) approaches. The worst performers over this range were the Suhs (SU) and multiple-wall (MW) models. This situation was reversed for the aft wall, with SU and MW performing best and SBL, ISU, LIA, REL, FL, and FP models performing poorly. This points to the fact that none of these models provide adequate surface pressure results over the entire cavity.

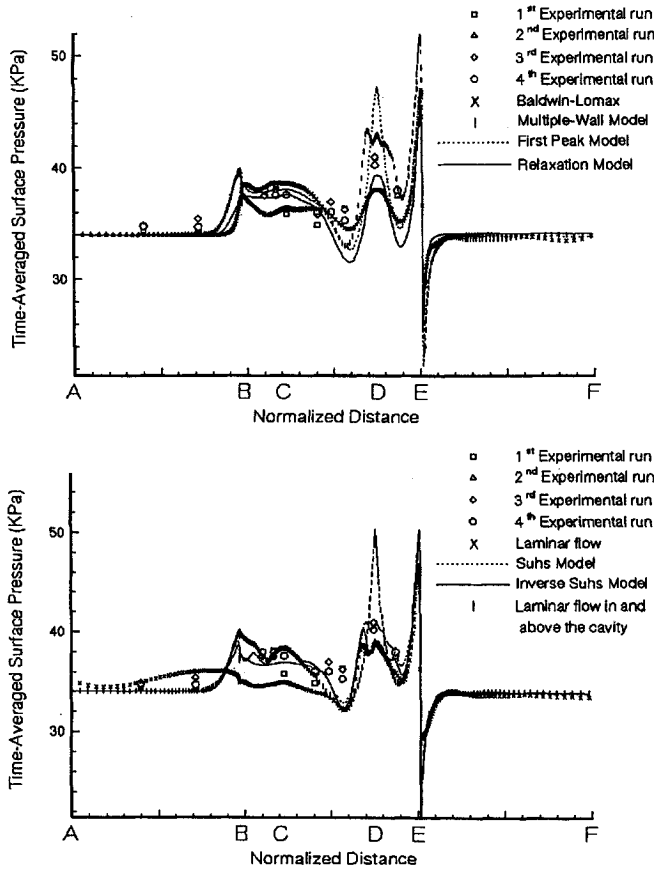

Fig. 2 Time-averaged surface pressure.

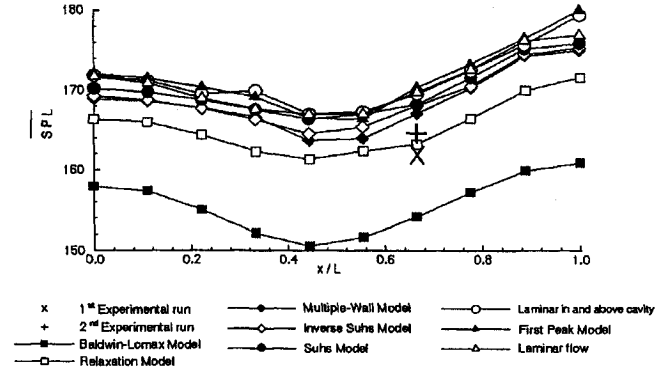

Fig. 3 Time-averaged sound pressure levels along the cavity floor.

In general, the results do not differ greatly between models. In fact, even the FL computation performed reasonably well on the aft wall. The FL result, however, contained the most oscillations, whereas the SBL result varied in the smoothest fashion. This is a consequence of the turbulent viscosity levels and will be discussed subsequently in greater detail.

Sound Pressure Level

The time histories of the surface pressures were recorded and used to form the time averaged sound pressure level ($\overline{SPL}$) along the cavity floor, which is computed by the equation

$$\overline{SPL} = 10 \log_{10} \left(\overline{p'^2} / p_{\text{ref}}^2 \right) \tag{1}$$

where

$$\overline{p'^2} = \frac{1}{T} \int_{T_1}^{T_2} (p - \bar{p})^2 \, dt \tag{2}$$

and p_{ref} is the standard reference value, 20 μPa. The comparison with experimental data shown in Fig. 3 at $\frac{2}{3}X/L$ along the cavity

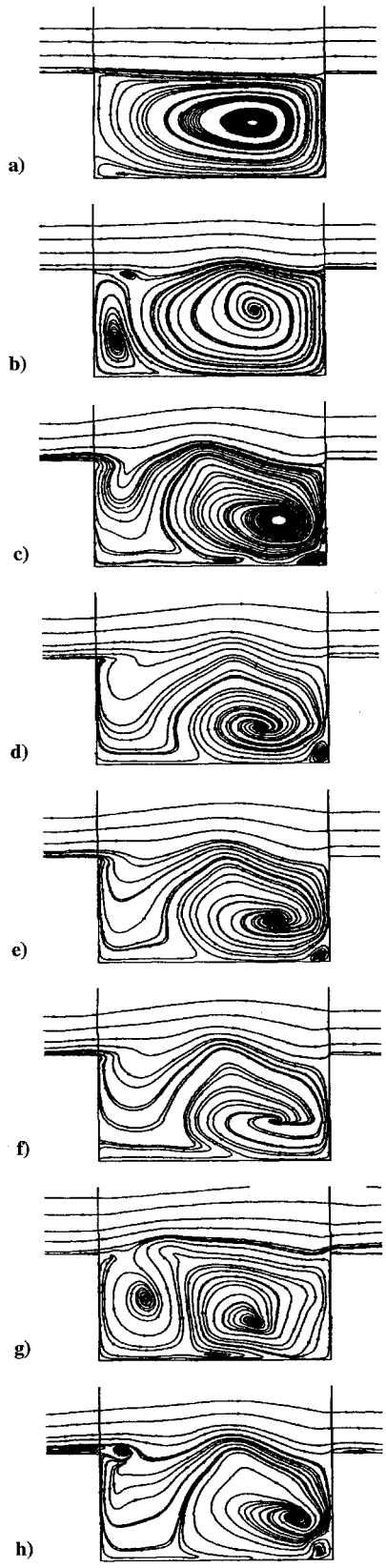

Fig. 4 Streamlines at time of maximum aft pressure: a) SBL, b) REL, c) ISU, d) SU, e) MW, f) FP, g) LIA, and h) FL.

floor shows that the REL results agreed best. All of the other approaches were at least 3 dB from the experimental values, with the SBL giving the maximum difference of 8 dB.

The surface property results provide clues as to the behavior of the respective turbulence models. It can be conjectured that turbulent viscosity plays an significant role in both the $\bar{p}$ and $\overline{SPL}$ results. Smoother $\bar{p}$ and lower $\overline{SPL}$ values were obtained as the viscous dissipation increased. This general trend is also reflected in the streamline results.

Streamlines

Instantaneous streamline results are quite useful in sorting out the behavior of the respective models and further establishing the effect of viscosity. Figure 4 illustrates the streamlines for each model plotted at the time of maximum center aft wall pressure. Note that in all cases, mass ingestion can be observed at the aft cavity wall. The general trends show that increasing viscosity decreases the number of vortices resident in the cavity and the frequency of vortex shedding.[6] Figure 4a shows a distinctly different flowfield topology for the SBL model when compared to the lower viscosity models. In contrast, Fig. 4f shows a wealth of vortices and, indeed, inflow separation for the FL case. Results between these extremes are quite similar. A left-hand-side secondary vortex appears to various degrees in all plots. Corner vortices appear in several cases.

Summary

A study of several modified versions of the Baldwin–Lomax turbulence model applied to two-dimensional supersonic open cavity flowfields was performed. The results were clearly affected by the levels of turbulent viscosity imposed in the cavity. The standard Baldwin–Lomax model was found to be the most dissipative and produced the worst overall performance, even when compared to fully laminar computations. The general effect of increased viscosity was a reduction in dominant frequency and overall cavity sound pressure levels. Elimination of turbulent viscosity led to increased resident vortices and unacceptably high-dominant frequencies. The tuned damping offered by many of the modifications produced considerable improvements. Although no model performed best in all areas, the multiple-wall modification provided the best compromise. Combinations of the models might produce a better result.

Acknowledgments

The authors wish to thank the U.S. Air Force Office of Scientific Research and Leonidas Sakell for their generous support through Grant F49620-93-0081. Computational resources were provided by the U.S. Army Waterways Experimental Shared Resource Center.

References

[1]Suhs, N. E., "Computations of Three-Dimensional Cavity Flow at Subsonic and Supersonic Mach Numbers," AIAA Paper 87-1208, June 1987.

[2]Rizzetta, D. P., "Numerical Simulation of Supersonic Flow Over a Three-Dimensional Cavity," *AIAA Journal*, Vol. 26, No. 7, 1988, pp. 799–807.

[3]Bradshaw, P., "Effects of Streamline Curvature on Turbulent Flow," AGARDograph 169, AGARD-AG-169, Aug. 1973.

[4]Baysal, O., Yen, G. W., and Fouladi, K., "Navier–Stokes Computations of Cavity Aeroacoustics With Suppression Devices," *Journal of Vibration and Acoustics*, Vol. 116, Jan. 1994, pp. 105–112.

[5]Degani, D., and Schiff, L. B., "Computation of Turbulent Supersonic Flows around Pointed Bodies Having Crossflow Separation," *Journal of Computational Physics*, Vol. 66, Sept. 1986, pp. 173–196.

[6]Tam, C.- J., Orkwis, P. D., and Disimile, P. J., "A Comparison of Several Standard Turbulence Models for 2-D Open Cavity Flow Field Computations," AIAA Paper 95-0361, Jan. 1995.

[7]Disimile, P. J., and Orkwis, P. D., "The Effect of Yaw Angle on the Dominant Frequencies of Rectangular Cavities in Supersonic Flow," *AIAA Journal* (to be submitted).

[8]Whitfield, D. L., "Implicit Upwind Finite Volume Scheme for the Three-Dimensional Euler Equations," Mississippi State Univ. Rept. MSSU-EIRS-ASE-85-1, Sept. 1985.

[9]Simpson, L. B., and Whitfield, D. L., "Flux Difference Split Algorithm for Unsteady Thin-Layer Navier–Stokes Solution," *AIAA Journal*, Vol. 30, No. 4, 1992, pp. 914–922.

[10]Orkwis, P. D, Tam, C. J., and Disimile, P. J., "Observations on Using Experimental Data as Boundary Conditions for Computations," *AIAA Journal*, Vol. 33, No. 1, 1995, pp. 176–178.